MIEC-type ceramic membranes for the oxygen separation technology

Konrad Świerczek[1,2*], *Hailei* Zhao[3,4,**], *Zijia* Zhang[1,3], and *Zhihong* Du[1,3]

[1]AGH University of Science and Technology, Faculty of Energy and Fuels, al. A. Mickiewicza 30, 30-059 Krakow, Poland
[2]AGH Centre of Energy, AGH University of Science and Technology, ul. Czarnowiejska 36, 30-054 Krakow, Poland
[3]University of Science and Technology Beijing, School of Materials Science and Engineering, Beijing 100083, China
[4]The Beijing Municipal Key Laboratory of New Energy Materials and Technologies, Beijing 100083, China

Abstract. Mixed ionic-electronic conducting ceramic membrane-based oxygen separation technology attracts great attention as a promising alternative for oxygen production. The oxygen-transport membranes should not only exhibit a high oxygen flux but also show good stability under CO_2-containing atmospheres. Therefore, designing and optimization, as well as practical application of membrane materials with good CO_2 stability is a challenge. In this work, apart from discussion of literature data, authors' own results are provided, which are focused on material-related issues, including development of electrode materials exhibiting high ionic and electronic conductivities.

1 Introduction

For centuries, oil, coal and other fossil fuels have been extensively used by humans in energy and transportation sectors, which over the time brought serious worldwide-scale environmental issues. Research for alternatives, to replace the traditional energy resources, is currently one of the major topics conducted in leading laboratories throughout the world. Membrane technology, which was successfully commercialized in many different industrial applications, including treatment of chemicals, food, gas, water, wastewater and pharmaceuticals [1-7], recently emerged as having a great potential also in clean and renewable power applications [8, 9]. Especially, application of dense ceramic membranes having mixed ionic-electronic conductivity (MIEC) is considered as a very attractive, alternative method for oxygen production, which is due to a relatively simple processing, continuous operation, perfect selectivity, as well as good efficiency [10]. During the operation, there are ionic and electronic fluxes involved, and oxidation and reduction reactions occur over the opposite surfaces of the dense membrane [11,12]. Microscopic description of the electrochemical processes includes several steps: (1) preferential

* Corresponding author: xi@agh.edu.pl
** Corresponding author: hlzhao@ustb.edu.cn

adsorption of O_2 molecules on the surface of the membrane; (2) dissociation of the molecule and charge transfer (reduction of O to O^{2-}); (3) diffusion of the oxygen anions through the dense material; (4) oxidation and association of O_2; and (5) desorption of oxygen molecules, respectively. Each of the steps can be limiting, and consequently, not only ionic and electronic conductivities of the material should be enhanced, but also catalytic activity toward oxygen reduction and oxidation. Apart from good transport properties, structural and chemical stability, also in CO_2-containing atmospheres, is of a crucial importance considering application of the MIEC-type ceramic membranes.

In this work, an overview of the current state-of-the-art candidate membrane materials, as well as most important issues, which need to be solved for the successful, further development of the MIEC-type ceramic membrane technology, are presented. Apart from commonly applied $ABO_{3-\delta}$ perovskite-type oxides, alternative layered $A_2BO_{4\pm\delta}$ compounds are discussed in more details. Results concerning a novel group of oxides having $(Ln_{2-x}A'_x)_{1-y}Ni_{1-z}B'_zO_{4\pm\delta}$ (Ln - selected lanthanides; A' - Sr, Ba; B' - selected 3d metals, e.g. Cu; In, Ga) formula are given, which due to the moderate values of the thermal expansion, good stability and high values of the mixed ionic-electronic conductivity are of a particular interest for the application. The A-site deficiency, as well as the B-site doping strategies are shown to allow enhanced oxygen flux through the membranes.

2 Application of MIEC-type ceramic membranes

Dense MIEC-type ceramic membranes play a vital role for production of a high purity hydrogen and oxygen *via* gas separation route [13]. This is due to their unsurpassed chemical stability at elevated temperatures (600-1000 °C) in a wide range of gas atmosphere compositions (oxidizing, inert and reducing conditions), allowing for their application in environments that are detrimental to organic, silica, palladium or other membranes, as well as due to the high values of ionic flux, achievable above 600 °C through oxide-based membranes.

The application of ceramic membranes in gas separation technology is important, and still under development [2, 9]. Specifically, using such a membrane, oxygen can be preferentially transferred from gas mixture (i.e. air), as depicted in Fig. 1, allowing to obtain high-purity oxygen for further usage, for example, for oxy-combustion processes, but also for production of medical-grade oxygen gas. Similarly, other gases can be separated from their mixtures, such as hydrogen using hydrogen-permeable membrane.

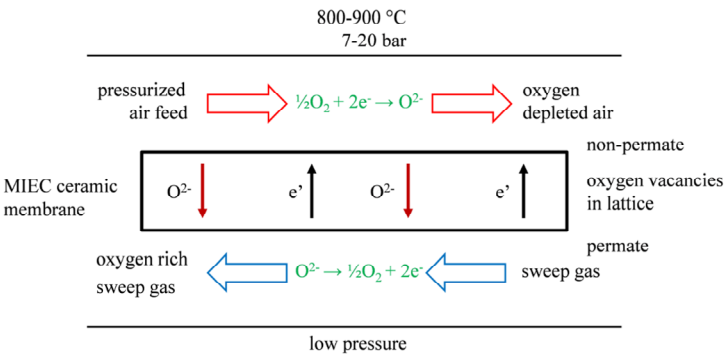

Fig. 1. Oxygen separation on MIEC-type membrane, based on [2, 6].

3 MIEC-type ceramic membranes

In all of the processes described above, there are ionic and electronic fluxes involved, and oxidation and reduction reactions occur over the opposite surfaces of the dense membrane [11, 12]. The driving force for the ionic transport is oxygen partial pressure difference at both sides of the membrane, which induces the chemical potential gradient across the membrane (Fig. 2). To maintain the electroneutrality, obviously there has to also transport of electrons and/or electron holes. Of importance, there is no need for any external electrodes and circuits for operation of such the membrane. Concerning influence of thickness of the membrane, it is known that diffusion-limited regime becomes surface kinetics-limited one with a decreasing of thickness below a certain level, which depends on the intrinsic values of the (bulk) chemical diffusion coefficient D and the surface exchange coefficient k [xx].

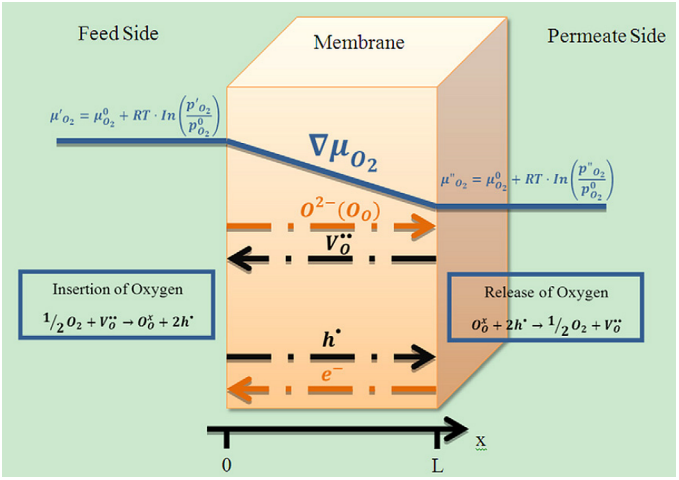

Fig. 2. Schematic representation of the ionic and electronic fluxes through the MIEC-type membrane with gradient of the chemical potential of oxygen marked, as the driving force [xx].

4 Perovskite- and Ruddlesden-Popper-based MIEC conductors

Majority of oxides exhibiting high mixed ionic-electronic transport possess either perovskite-type or perovskite-related (e.g. Ruddlesden-Popper-type) crystal structure [14-16]. In the $A_{n+1}B_nO_{3n+1}$ series, ABO_3 perovskite materials can be considered as an end-member with $n = \infty$, while for $1 \leq n < \infty$ the structure corresponds to Ruddlesden-Popper-type series. This type of crystal contains perovskite-like layers separated by rock salt-like layers. The most important member of this family is A_2BO_4 compound ($n = 1$), with its unit cell shown in Fig. 3.

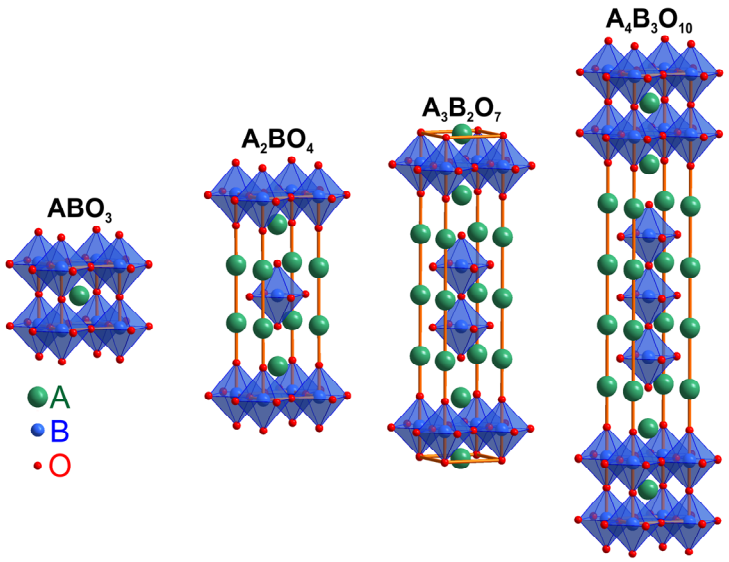

Fig. 3. Visualization of selected compounds from $A_{n+1}B_nO_{3n+1}$ series, based on [17].

In stoichiometric ABO_3 perovskite, B-site cations are present in the octahedral coordination, while larger A-site cations are surrounded by 12 ligands. A and O atoms form cubic-like close packing, and therefore, no interstitial sites are available for the oxygen [12, 16, 18-20]. Interestingly, in the Ruddlesden-Popper series interstitial sites for the oxygen anions are available in the rock salt layers, and this property allows for unique, interstitial-type of the ionic transport.

In whole $A_{n+1}B_nO_{3n+1}$ series, electronic component of the electrical conductivity is governed by the double exchange mechanism (B-O-B) with an essential contribution from oxygen, which *p*-orbitals ought to overlap effectively with *d*-orbitals of transition metal (B-site) cation for effective charge transport. Because transfer integral $I_{p\text{-}d}$ is proportional to cosine of B-O-B angle, the most favorable situation occurs when crystal symmetry is cubic (Fig. 4). In the case of Ruddlesden-Popper-type oxides, mechanism of the charge transport is essentially the same, but as the perovskite layers form 2-dimentional network, the transport occurs in layers, with only small perpendicular contribution [13, 21, 22].

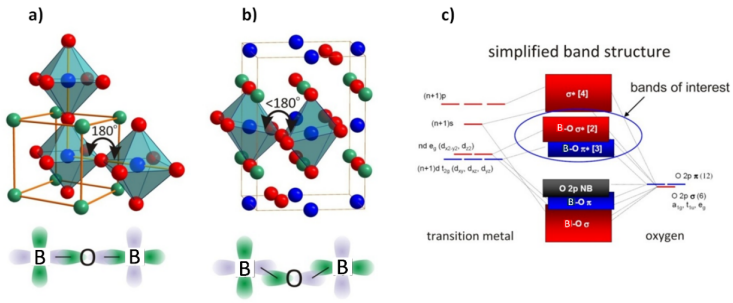

Fig. 4. (a) Effective overlapping of *d* and *p* orbitals in cubic (space group *Pm-3m*) perovskite-type oxide, (b) less-effective overlapping of orbitals in distorted (e.g. orthorhombic *Pnma*) structure, (c) simplified band structure of ABO_3 perovskite.

Crystal structure of the perovskite-type ABO_3 material can be discussed on a basis of so called Goldschmidt tolerance factor *t*, defined in Eq. 1 [23, 24]:

$$t = (r_A+r_O)/\sqrt{2}(r_B+r_O) \quad (1)$$

where r_A, r_B and r_O stand for respective ionic radii. Interestingly, the above equation can be used to analyze structural characteristic of A_2BO_4 compounds as well [25, 26]. However, several other parameters were introduced to predict transformation from K_2NiF_4-type to Nd_2CuO_4-type structure. Tolerance factor *t* is widely used for an initial prediction of possibility of formation of the perovskite (or A_2BO_4) structure, and may help to evaluate magnitude of the structural distortion, which is known to increase with a decreasing value of *t* [22]. With the increasing structural distortion, a continuous or non-continuous change of the crystal symmetry occurs. Because temperature change of force constant is smaller for A-O bond than for B-O bond, tolerance factor *t* increases at elevated temperatures. This leads to alleviation of the structural distortion, but may also cause an appearance of the unwanted phase transition on heating, which in the case of the 1st order phase transformation induces detrimental mechanical stress in the material.

Ionic transport in perovskite-type $ABO_{3-\delta}$ oxides is realized by the oxygen vacancy (δ) mechanism, with stress-free lattice, cubic symmetry ($t \approx 1$), low mean value of metal-oxygen bonding energy, as well as large critical radius r_c (Fig. 5) being the dominant factors ensuring high ionic conductivity [27, 28]. Usually, the ionic conductivity is at least 100-1000 times smaller than the electronic one, for transition metal ions B with electronic configuration other than d^0 [29]. In regards to the oxygen sublattice, $A_2BO_{4\pm\delta}$ materials can be either hypo- or hyper-stoichiometric, with oxygen vacancies or interstitial oxygen defects, respectively.

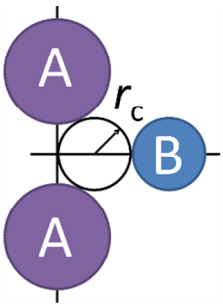

Fig. 5. Critical radius r_c for ionic movement in $ABO_{3-\delta}$ perovskites [27].

In an aspect of bulk materials, perovskite-related (layered) $A_2BO_{4\pm\delta}$ oxides exhibit conventional oxygen vacancy-type oxygen transport mechanism ($\delta < 0$) or a unique interstitial-type transport ($\delta > 0$) [30-33]. In the former case, the ionic transport is similar to the case of $ABO_{3-\delta}$ materials, however, in the latter case, interstitial oxygen is known to diffuse in the rock salt layers $A_2O_{2\pm\delta}$, yet this transport is 2-dimentional (within the layers). The interstitial oxygen transport is of a great interest for modern solid state chemistry and physics, as such ionic transport occurs with an unusually low activation energy, and may allow to manufacture MIEC membranes with superb properties.

Chemical composition of such the proposed $A_2BO_{4\pm\delta}$ compounds can be generally written as $(Ln_{2-x}A'_x)_{1-y}Ni_{1-z}B'_zO_{4\pm\delta}$ (Ln - selected lanthanides; A' - Sr, Ba; B' - selected 3d metals), where *x* represents degree of substitution in the A-sublattice by +2 cations ($Ln_{2-x}A'_x$), *y* stands for the cationic nonstoichiometry in the A-sublattice, and *z* corresponds

to substitution in the B-sublattice ($Ni_{1-z}B'_z$) by different 3*d* metals. As mentioned above, values of the oxygen nonstoichiometry δ are expected to be above (interstitial oxygen) or below (oxygen vacancies) zero, depending on the overall chemical content of the compound.

5 Overview of Ruddlesden-Popper-type membranes

Among layered materials with A_2BO_4 structure, Ni-containing oxides have been already shown as promising candidates for MIEC oxygen transporting membranes, however, the reported flux values were so far not very impressive [34-36]. Only recently, a significant progress was achieved for such compounds, and it was realized by an introduction of the A-site nonstoichiometry, as well as by the B-site doping with Ga^{3+} in Ni-rich $(Pr_{0.9}La_{0.1})_{1.9}Ni_{0.74}Cu_{0.21}Ga_{0.05}O_4$ ($PL_{1.9}NCG$) [37]. As shown in the Fig. 6, membrane prepared using cation-nonstoichiometric $PL_{1.9}NCG$ allowed to obtain significantly higher oxygen flux, comparing to $PL_{1.9}NCG$ sinter, which is cation-stoichiometric PL_2NCG [37]. It should be pointed out that the deficiency in the A-site is considered to facilitate the oxygen vacancy transport mechanism, which is realized by a transfer between two adjacent apical sites, enhancing performance (oxygen flux) of the discussed membrane [37]. Also, due to a lack of Sr and Ba in the composition, very good stability in CO_2-containing atmospheres of such the candidate membrane material was observed, and this can be also expected for other layered A_2BO_4 nickelates and cuprates. So far, possibility of similar doping was not thoroughly studied in the Cu-rich layered oxides.

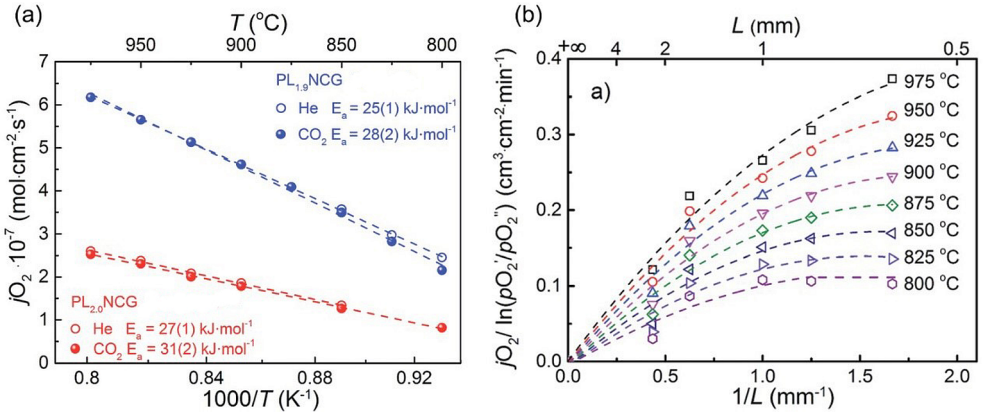

Fig. 6. (a) Temperature dependence of the oxygen permeation flux reported for cation nonstoichiometric $PL_{1.9}NCG$ and cation-stoichiometric PL_2NCG. (b) Dependence of the normalized oxygen flux on the inverse membrane thickness for the elaborated $PL_{1.9}NCG$ [37]. Used with permission.

6 Cu-based Ruddlesden-Popper-type membranes

Possibility of modification of Cu-based, layered oxides with K_2NiF_4-type structure is studied concerning formation of cationic nonstoichiometry in the A-sublattice, as well as by introduction of selected M^{3+} cations (Sc, Ga, In) at the B-site into the parent La_2CuO_4. It is shown that synthesis of phase-pure $La_{2-x}CuO_4$ can be done with values of $x \leq 0.1$, and in the A-site nonstoichiometric materials further doping with M^{3+} is also achievable [38]. Formation of solid solutions for M^{3+}-doped samples follows the expected trend, with the

widest range observed for the smallest Sc^{3+} cation, $z \leq 0.1$. Apart from a different structural behaviour of the doped oxides at high temperatures, it is documented that the discussed substitution affects strongly the oxygen content (e.g. high concentration of the oxygen vacancies in $La_{1.9}CuO_{3.87}$), as well as electrical conductivity.

The electronic conductivity of the investigated samples is shown in Fig. 7. In comparison to La_2CuO_4 [39], a lower electrical conductivity is observed for $La_{1.9}CuO_{3.87}$, but the same temperature behaviour can be seen. However, with Sc-doped sample, $La_{1.9}Cu_{0.9}Sc_{0.1}O_{3.93}$, higher electrical conductivity was measured in the intermediate temperature range. Moreover, its electronic conductivity increases with temperature up to ca. 450 °C and follows a linear relationship, implying that the small polarons take a conductive role via B-O-B transmission paths [40, 41]. After reaching the highest point, the electrical conductivity begins to decrease due to the release of lattice oxygen, which is likely caused by annihilation of electron holes and generation of oxygen vacancies [42-44]. For sample with $La_{1.9}Cu_{0.45}Ni_{0.45}Sc_{0.1}O_{3.98}$ composition the oxygen release occurs at lower temperatures compared with $La_{1.9}Cu_{0.9}Sc_{0.1}O_{3.93}$. In the intermediate range, its conductivity values are higher than for the undoped samples. This is good result indicating that further improvement can be done by adjusting doping level and Ni-Cu ratio.

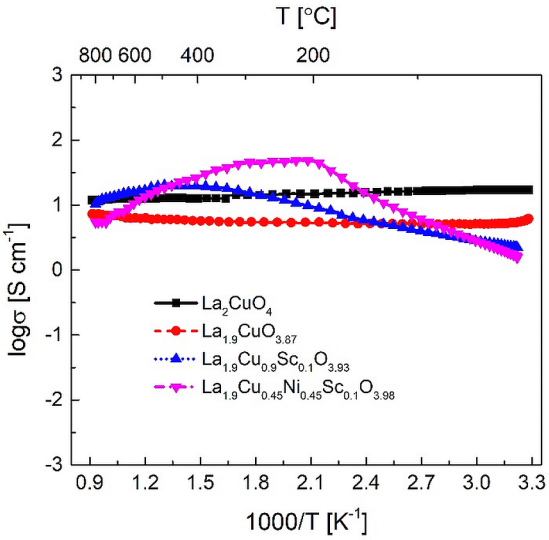

Fig. 7. Temperature dependence of the electrical conductivity for the investigated samples in air.

The permeation performance of 1 mm thick $La_{1.9}Cu_{0.9}Sc_{0.1}O_{4-\delta}$ membranes under the conditions of 60/120 mL min^{-1} He/air from 800 °C to 950 °C was also measured. The recorded oxygen permeation fluxes as a function of temperature are shown in Fig. 8. With increasing temperature, the oxygen permeation fluxes of the sample increase gradually. It is due to the enhancement of oxygen bulk diffusion and oxygen surface reaction rates, as well as increased oxygen vacancy concentrations. The oxygen permeation flux achieves a maximum of 0.37 mL min^{-1} cm^{-2} at 950 °C. Comparing to the unmodified $La_2CuO_{4-\delta}$ membrane and reported work with data for $(Pr_{0.9}La_{0.1})_{1.9}Ni_{0.74}Cu_{0.21}Ga_{0.05}O_{4-\delta}$ oxide [37], the oxygen fluxes in this work are much higher, nearly two times. The oxygen permeation fluxes for both Cu-based membranes increase linearly in Arrhenius-type coordinates in high temperature range, and calculated the activation energy for oxygen ion migration (E_a) is ca. 0.3 eV.

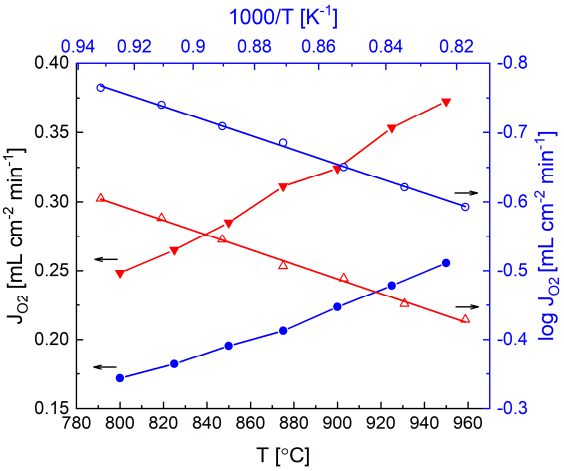

Fig. 8. Temperature dependence of the oxygen permeation flux through the 1 mm thick $La_{1.9}Cu_{0.9}Sc_{0.1}O_{4-\delta}$ membrane (full and empty triangles). For comparison, data for unmodified $La_2CuO_{4-\delta}$ are also given (full and empty circles).

7 Summary

MIEC-type ceramic membranes, including $A_2BO_{4\pm\delta}$ oxides, seem as a promising choice for gas separation. However, there are still material-related issues needs to be addressed before their practical application. This includes development of membrane materials exhibiting high ionic-electronic conductivity. It seems that it is achievable by a proper selection of composition of the compounds and composites.

Acknowledgements. The project was funded by the National Science Centre, Poland on the basis of the decision number UMO-2015/19/B/ST8/00871.

References

1. A. Basile, S.P. Nunes (Editors), *Advanced Membrane Science And Technology For Sustainable Energy And Environmental Applications,* (Woodhead Publishing Limited, 2011)
2. K. Li, *Ceramic Membranes For Separation And Reaction*, (John Wiley & Sons Ltd, 2007)
3. A. Basile, *Handbook Of Membrane Reactors*, (Woodhead Publishing Limited, 2013)
4. E. Drioli, G. Barbieri (Editors), *Membrane Engineering For The Treatment Of Gases Volume 1: Gas-Separation Problems With Membranes*, (Royal Society Of Chemistry, 2011)
5. E. Drioli, G. Barbieri (Editors), *Membrane Engineering For The Treatment Of Gases Volume 2: Gas-Separation Problems Combined With Membrane Reactors,* (Royal Society Of Chemistry, 2011)
6. Y. Yampolskii, B. Freeman, *Membrane Gas Separation,* (John Wiley & Sons Ltd, 2010)
7. R.W. Baker, *Membrane Technology And Applications*, (John Wiley & Sons Ltd, 2012)
8. A. Gugliuzza, A. Basile (Editors), *Membranes For Clean And Renewable Power Applications,* (Woodhead Publishing Limited, 2014)

9. V.V. Kharton (Editor), Solid State Electrochemistry II: Electrodes, Interfaces And Ceramic Membranes, Wiley-Vch Verlag & Co. KGaA, 2011
10. R. Kneer, D. Toporov, M. Förster, D. Christ, Energy Environ. Sci. **3** (2010)
11. K. Zhang, L. Ge, R. Ran, Z. Shao, S. Liu, Acta Mater. **56** (2008)
12. C. Li, K.C.K. Soh, P. Wu, J. Alloy Compd. **372** (2004)
13. H.J.M. Bouwmeester, A.J. Burggraaf, Amsterdam: Elsevier Science B **V** (1996)
14. S. Takahashi, S. Nishimoto, M. Matsuda, M. Miyake, J. Am. Ceram. Soc. **93** (2010)
15. A. Aguadero, J.A. Alonso, M.J. Escudero, L. Daza, Solid State Ion. **179** (2008)
16. F. Pradoa, N. Grunbaum, A. Caneiro, A. Manthiram, Solid State Ion. **167** (2004)
17. R.H. Mitchell, *Perovskites Modern and Ancient*, (Almaz Press Inc. 2002)
18. H.J.M. Bouwmeester, Catal. Today **82** (2003)
19. T. Nagai, W. Ito, T. Sakon, Solid State Ion. **177** (2007)
20. Z. Deng, W. Yang, W. Liu, C.S. Chen, J. Solid State Chem. **179** (2006)
21. J.H. Lee, G. Luo, I.C. Tung, et al., Nature Mater. **13** (2014)
22. A.C. Tomkiewicz, M. Tamimi, A. Huq, S. McIntosh, J. Mater. Chem. A **3** (2015)
23. J.A. Kilner, R.J. Brook, Solid State Ion. **6** (1982)
24. A.F. Sammells, R.L. Cook, J.H White, J.J. Osborne, R.C. MacDuff, Solid State Ion. **52** (1992)
25. H. Kruidhof, H.J.M. Bouwmeester, R.H.E. Doorn, A.J. Burggraaf, Solid State Ion. **63** (1993)
26. D.N. Mueller, R.A. De Souza, T.E. Weirich, D. Roehrens, J. Mayer, M. Martin, Phys. Chem. Chem. Phys. **12** (2010)
27. T. Ishihara, *Perovskite Oxide for Solid Oxide Fuel Cells,* (Springer, 2009)
28. M. Mogensen, D. Lybye, N. Bonanos, P.V. Hendriksen, F.W. Poulsen, Solid State Ion. **174** (2004)
29. Y. Teraoka, H.M. Zhang, K. Okamoto, N. Yamazoe, Mater. Res. Bull. **23** (1988)
30. V.A. Alyoshin, I.P. Romanova, D. Mikhailova, S. Oswald, A. Senyshyn, H. Ehrenberg, J. Phys. Chem. A **114** (2010)
31. B.B. He, G. Li, Q. Gui, Y.H. Ling, L. Zhao, J. Mater. Chem. A **4** (2016)
32. W. Fang, F. Liang, Z. Cao, et al., Angew. Chem. Int. Ed. **54** (2015)
33. E.V. Tsipis, V.V. Kharton, J. Solid State Electrochem. **12** (2008)
34. D.C. Zhu, X.Y. Xu, S.J. Feng, W. Liu, C.S. Chen, Catal. Today **82** (2003)
35. J.B. Smith, T. Norby, J. Electrochem. Soc. **153** (2006)
36. V.V. Kharton, A.P. Viskup, E.N. Naumovich, F.M. B. Marques, J. Mater. Chem. **9** (1999)
37. J. Xue, Q. Liao, W. Chen, et al., J. Mater. Chem. A **3** (2015)
38. Z. Zhang, Z. Du, A. Niemczyk, K. Li, H. Zhao, K. Świerczek, Solid State Ionics **317** (2018)
39. K. Zheng, A. Gorzkowska-Sobaś, K. Świerczek, Mater. Res. Bull. **47** (2012)
40. J.B. Goodenough, Rep. Prog. Phys. **67** (2004)
41. C. Zener, Phys.Rev. **82** (1951) 403
42. Y. Lu, H. Zhao, X. Chang, X. Du, K. Li, Y. Ma, S. Yi, Z. Du, K. Zheng, K. Świerczek, J. Mater. Chem. A **4** (2016)
43. Y. Lu, H. Zhao, K. Li, X. Du, Y. Ma, X. Chang, N. Chen, K. Zheng, K. Świerczek, J. Mater. Chem. A **5** (2018)
44. K. Li, H. Zhao, Y. Lu, Y. Ma, Z. Du, Z. Zhang, J. Membrane Sci. **550** (2018)